Effects of Core-modification on Porphyrin Sensitizers to the Efficiencies of Dye-sensitized Solar Cells

Sandeep B. Mane,[a,b] Liyang Luo,[c] Gao-Fong Chang,[a] Eric Wei-Guang Diau[d] and Chen-Hsiung Hung[a],*

[a]*Institute of Chemistry, Academia Sinica, Nankang Taipei 115, Taiwan.*
[b]*Department of Chemistry, National Taiwan Normal University, Taipei 116, Taiwan.*
[c]*Department of Chemistry, Chung Yuan Christian University, Chung Li 320, Taiwan.*
[d]*Department of Applied Chemistry, National Chiao Tung University, Hsinchu 300, Taiwan.*

To study dye-sensitized solar cells (DSSCs) with core-modified porphyrins as the sensitizing dyes, three porphyrins with an ethynyl benzoic acid as an anchoring group are prepared. The properties of free-base regular porphyrin (N4), thiaporphyrin (N3S) and oxaporphyrin (N3O) were thoroughly studied by spectroscopic methods, DFT calculations, and photovoltaic measurements. Replacing one of the porphyrinic core nitrogen atoms by oxygen or sulfur considerably changes the absorption spectra. The *Soret* band of the N3O and N3S observed bathochromic shifts of 3-9 nm while the *Q* band reaches 700 nm to the near-infrared region. The overall conversion efficiencies of the DSSCs based on these porphyrins are in the order N4 (3.66%) >> N3S (0.22%) > N3O (0.01%). The time-correlated single photon counting observed short fluorescence lifetimes for N3O adsorbed both on TiO_2 and Al_2O_3 which explicates the poor efficiency of DSSC using N3O as the photosensitizer.

Keywords: Core-modified porphyrins; Dye-sensitized solar cells; Photovoltaics.

INTRODUCTION

Production of eco-friendly and cost-effective energy is one of the major challenges for scientific community. Among the known renewable energy sources, solar energy is the most likely choice as it is abundant and sustainable. Dye-sensitized solar cell (DSSC) made from a crystalline TiO_2 electrode coated with a layer of photosensitizing dye is one of the most promising contenders in recent quest for cheaper, cleaner and greener alternatives to fossil fuels.[1] The overall solar energy conversion efficiencies of dye molecules can be strongly influenced by light harvesting properties of the sensitizing dyes, electronic structure and photophysical properties of dyes,[1e,2] anchoring group of the dyes,[3] bridging distance between the dye and TiO_2,[4] and type of the central metal.[5] Amid these factors, light harvesting properties of the dye molecules are the most important. In recent years, a variety of sensitizers including ruthenium complexes, porphyrins, phthalocyanines, and organic dyes have been studied extensively to find a cost effective and highly efficient sensitizer.[1e,2,6] The ruthenium sensitizers had achieved the best conversion efficiency of 11.4% but their commercial applications are limited owing to low absorption coefficients of ruthenium dyes and limited resources of ruthenium metal.[7] Porphyrinic dyes have attracted much attention owing to their structural relationship with chlorophylls of the photosystem antenna complexes and their unique optical properties along with their photochemical and thermal stability.[6] In last decade, a wide variety of porphyrins has been extensively studied as sensitizers in DSSCs. The device based on the D-π-A push-pull zinc porphyrin sensitizer, YD2-*o*-C8, co-sensitized with an organic dye using a cobalt based redox electrolyte reached a benchmark efficiency of 12.3%.[8] Different molecular designs have been conducted to extend the absorption wavelengths of porphyrins to the near-infrared region in order to subsequently increase their overall photon to current conversion efficiencies. Two mostly explored routes to modify peripheral substituents of the porphyrin core are through either extending π-conjugation system over β- or *meso*-positions or fusing porphyrins with aromatic chromophores.[9] Alternatively, the replacement of one or more pyrrolic nitrogens on the porphyrin central core with heteroatoms is another important but less explored approach to push the absorption of porphyrins towards red region.[10] Our lab is interested in the synthesis of core modified porphyrins and their metal complexes.[11] We

---

have recently shown that oxasmaragdyrin boron complexes, which are a class of expanded core-modified porphyrin with 22 π-electrons, can be used as efficient sensitizers for DSSCs.[12]

The replacement of one or more pyrrolic nitrogens with the Group 16 heteroatoms like oxygen, sulfur, selenium, and tellurium in a porphyrin ring leads to a heteroatom substituted core-modified porphyrin.[13] This core perturbation results in significant changes in the optical, photophysical, electrochemical, magnetic, and metal binding properties while retains the aromatic character. Surprisingly, the application of the core-modified porphyrins in DSSC as a sensitizer is very rare. The only article which demonstrates the use of core-modified porphyrins as the sensitizing dye in DSSCs is reported by Xie *et al.* where *meso* 2-thienyl substituted mono- and di-thiaporphyrins were used as sensitizers to obtain the highest efficiency of 0.19%.[14] There is no report comparing the photophysical, electrochemical, and photovoltaic properties of regular and core modified porphyrins thus far.

One of the reasons for the low efficiency of the reported thiaporphyrin dyes-based DSSCs would be due to the lack of an effective electronic coupling between the porphyrin ring and the anchoring group to ensure an efficient charge transfer from the dye to TiO₂ semiconductor. In most of the highly efficient porphyrin dyes, ethynylphenyl group is used as a linker to couple the porphyrin ring and the anchoring carboxyl group.[8,9c] In this report, we have synthesized novel core-modified porphyrins, N3S and N3O, with an ethynylphenyl group as the anchoring group as shown in Scheme I to examine the effects of core atom modification on the photovoltaic properties in DSSCs. This systematic study elucidates the significant influence of core atom replacement on the electronic structure, photophysical, and photovoltaic properties. The photovoltaic study reveals that in spite of the broad absorption peaks of core-modified porphyrins covering some near-infrared region, the overall photon-to-current conversion efficiencies
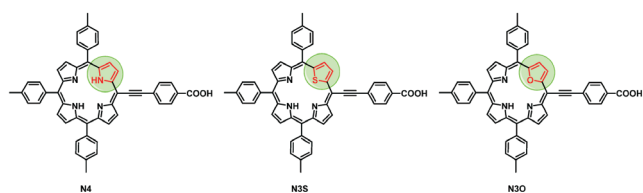
of these porphyrins are much lower than the regular porphyrins.

RESULTS AND DISCUSSION
Synthesis

The free-base porphyrins, N4, N3S, and N3O, were synthesized from readily accessible starting materials in two steps. The mono *meso*-unsubstituted regular porphyrin (1) was prepared by literature procedures. The thiaporphyrin (2) and oxaporphyrin (3) were prepared by condensation of thiophene or furan diol with two equivalents of tolualdehyde and three equivalents of pyrrole in presence of catalytic amount of boron trifluoride etherate. As shown in Scheme II, these mono *meso*-unsubstituted porphyrins were then treated with N-bromosuccinimide in dry dichloromethane to give 5-bromo substituted porphyrins in 70-78% yields. The *m/z* peaks in mass spectra and the disappearance of the *meso* proton signal in ¹H NMR spectra confirmed the identity of the bromoporphyrins. These bromoporphyrins were further reacted with 4-ethynylbenzoic acid in tetrahydrofuran and triethylamine at room temperature by Sonogashira coupling in presence of Pd₂(dba)₃ as the catalyst to obtain the desired 4-ethynylbenzoic acid substituted porphyrins (7)-(9) with moderate yields. In the ¹H NMR spectra of N3S and N3O porphyrins, it is observed that β-thiophene and β-furan protons appeared as two doublets. The downfield shifts of the β-pyrrolic protons and the inner NH in the heteroporphyrins compared to

Scheme II Synthesis of N4, N3S and N3O porphyrin. Reagents and conditions: i) BF₃·OEt₂, DDQ, CH₂Cl₂; ii) NBS, CH₂Cl₂, room temp.; iii) 4-Ethynylbenzoic acid, Pd(dba)₃, AsPh₃, THF, NEt₃, room temp.

Scheme I Molecular structures of the studied porphyrin dyes
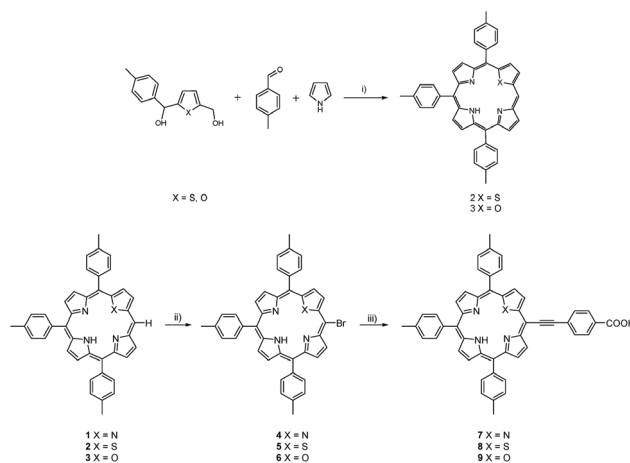
the N4 porphyrin confirms the core perturbation effect on porphyrin ring. The introduction of ethynyl bond between the porphyrin ring and the benzoic acid helps to maintain the planarity of the molecule assuring the effective electron coupling.

Optical Spectroscopy

The UV-visible peak positions of the *Soret* and *Q* bands and the molar absorption coefficients (ε) of N4, N3S and N3O in THF are listed in Table 1. The UV-visible spectra of the studied porphyrins as displayed in Figure 1, show typical features of free-base porphyrins, which consist of a strong *Soret* band around 450 nm and four *Q* bands around 520-700 nm. The core atom alteration results in slight red-shifts in the *Soret* as well as *Q* bands extending the absorption maximum beyond 700 nm. The molar absorption coefficients of N3S thiaporphyrin and N3O oxaporphyrin are slightly higher than regular N4 porphyrin.

To obtain the absorption spectra of the thin films, the TiO$_2$ films with coating thickness of 1 μm were immersed in THF solution of the porphyrins for 2 h at 40 ^{o}C and rinsed with THF to remove unadsorbed dye. The absorption spectra were recorded by reflectance measurements using an integrating sphere and the results are depicted in Figure 2. The examination on the *Soret* band region of spectra for dyes adsorbed on TiO$_2$ observed peak broadening for all compounds in comparison with the corresponding spectra in THF, which reflects significant degree of H-aggregation for all compounds on TiO$_2$. Noticeably, in the Q band region, the broadening of N3O/TiO$_2$ is more dramatic than that of N4/TiO$_2$ or N3S/TiO$_2$, which implies
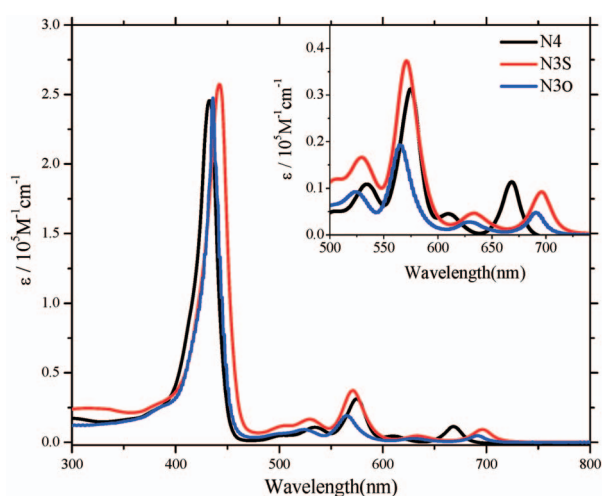
Table 1. Optical and Electrochemical data of N4, N3S, and N3O porphyrin in THF

Dye	λ_{abs}/nm[a] (ε/10^{3}M^{-1}cm^{-1})	λ_{em} nm[b]	Φ[c]	E_{ox} V[d]	$E_{(0,0)}$ eV[e]	E_{ox}* V[f]
N4	433 (245), 534 (11), 575 (31), 610 (4.5), 668 (11)	673	0.11	0.93	1.85	−0.92
N3S	442 (257), 529 (17), 571 (37), 633 (5), 696 (9)	704	0.02	0.96	1.77	−0.81
N3O	436 (247), 525 (9), 565 (19), 629 (3), 691 (5)	695	0.06	0.97	1.79	−0.83

[a] Absorption maximum of porphyrins in THF. [b] Emission maximum measured in THF by exciting at *Soret* band. [c] Relative quantum yields of the porphyrins were calculated with reference to TPP (Φ = 0.11 in toluene). [d] Oxidation potentials approximated from E_{ox}* and $E_{(0,0)}$. [e] $E_{(0,0)}$ values were estimated from the intersection of the absorption and emission spectra. [f] First reduction potentials vs. NHE determined by cyclic voltammetry in THF and referenced to the ferrocene redox couple.

a higher degree of aggregation for N3O than N4 and N3S when adsorbed on TiO$_2$.

The steady-state fluorescence spectra of all the core-modified porphyrins measured in THF by excitation at the *Soret* band wavelengths display the similar red-shifting as UV-vis spectra (Figure 3). These bathochromic shifts in the absorption and emission spectra of heteroporphyrins may be attributed to structural distortion of porphyrin π-system or the electronic effect of heteroatoms. From the density functional theory studies we observed negligible deviation from the planarity for the heteroporphyrins. Therefore, the red shifts in the spectra are more likely caused by the elec-
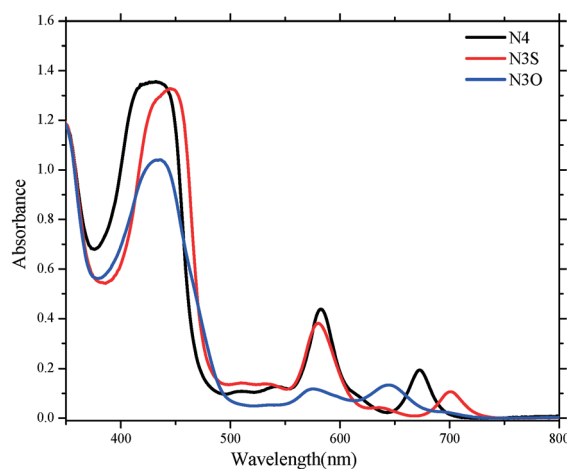

Fig. 1. UV-visible spectra of N4, N3S and N3O in THF. Inset shows enlarged spectra for *Q* band region.

Fig. 2. UV-visible spectra of N4/TiO$_2$, N3S/TiO$_2$ and N3O/TiO$_2$.

tronic effects of the heteroatoms.[10] We measured the relative quantum yields of all three porphyrins in THF with reference to the value of tetraphenylporphyrin and the results are depicted in Table 1. The decreased quantum yields for N3O and N3S suggest that the non-radiative decay rates of the internal conversion or the intersystem crossing are much faster for the heteroporphyrins compared to the regular porphyrins. The much lower quantum yield for N3S than those of N4 and N3O porphyrins indicates that the heavy atom effect of sulfur accelerates intersystem crossing rate.[15]

Cyclic Voltammetry

The cyclic voltammetry measurements of the porphyrins were carried out in degassed THF containing 0.1 M [Bu$_4$N]PF$_6$ as the supporting electrolyte to obtain the first reduction potentials. The reduction couples of the studied porphyrins show reversible redox processes under a scan rate of 50 mV/sec and are stable over multiple scans. As depicted in Table 1, the reduction potential of thiaporphyrin N3S (-0.81 V vs NHE) shifts positively by 110 mV and the oxaporphyrin N3O (-0.83 V vs NHE) also positively shifts by 90 mV as compared to regular N4 porphyrin (-0.92 V vs NHE) making them easier to be reduced. The zero-zero excitation energies, $E_{(0,0)}$ were calculated from the intersection of the normalized absorption and emission spectra at the $Q(0,0)$ band (See supporting information Figure S1) and were found to be 1.85, 1.77 and 1.79 eV for N4, N3S and N3O porphyrins, respectively. The oxidation potentials were estimated from the reduction potentials and the zero-zero excitation energies and are listed in Table 1. The energy level diagram for these porphyrins is displayed in
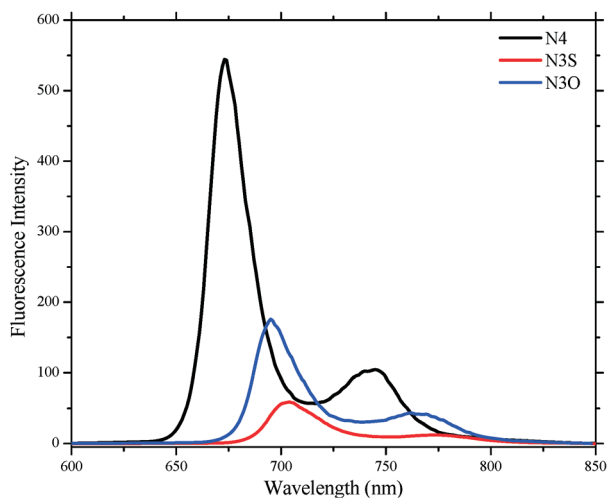
Figure 4. As shown in the figure, the lowest unoccupied molecular orbitals (LUMO) of the porphyrins are more negative than the TiO$_2$ conduction band and thus ensure enough driving force for the electron injection from the LUMO energy level of the dye to the TiO$_2$ conduction band. The highest occupied molecular orbitals (HOMO) of all the porphyrins are more positive than the redox electrolyte which confirms the efficient dye regeneration.

DFT Calculations

To correlate the molecular structures of the dyes with the performance of DSSCs, DFT as well as TD-DFT calculations were carried out. The results from quantum chemical calculations show planar macrocycles for all the porphyrins as shown in Figure 5. In HOMO of all the porphyrins, the majority of the electron density is localized on the porphyrin ring however a small portion is also extended over the ethynylphenyl group, while in the LUMO the elec-
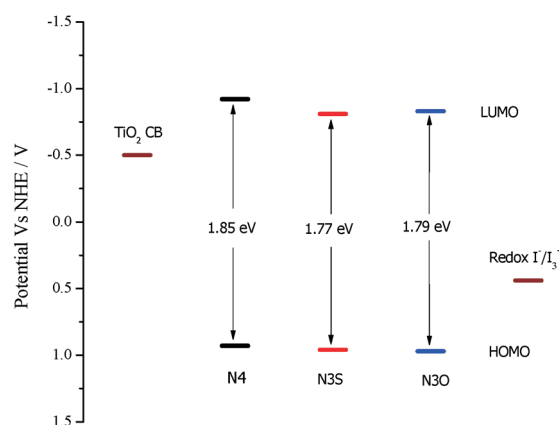

Fig. 4. Energy level diagram for the studied porphyrin dyes.

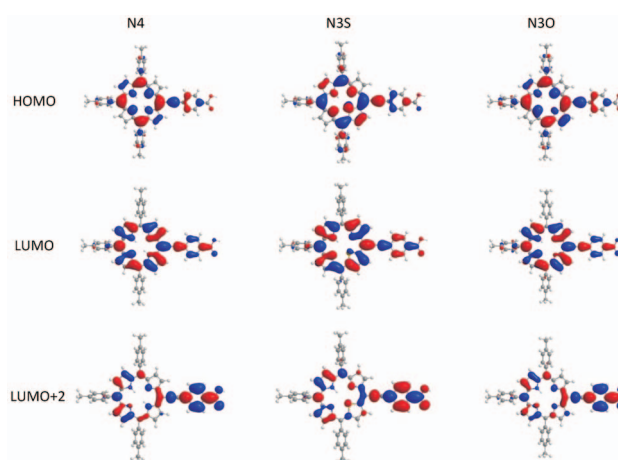Fig. 3. Fluorescence spectra of porphyrin dyes in THF.

Fig. 5. Molecular orbital diagrams of N4, N3S and N3O obtained from DFT calculations.

tron density is populated equally on the porphyrin ring and the ethynylbenzoic acid acceptor. The increased electron density populating to the anchoring group in the LUMO facilitates efficient charge transfer from the excited state of the porphyrins to the TiO$_2$ conduction band. Interestingly in the LUMO+2, the electron density is extensively located on the ethynylbenzoic acid acceptor suggesting that the electron injection from the higher excited states involving LUMO+2 might be more efficient than LUMO.

It is evident from TD-DFT calculations that the calculated wavelengths given in Table 2 are in good agreement with the experimental values. Pointedly the calculations obtained dipole moments for the studied porphyrins in order, N4 > N3S > N3O. This trend is similar with the overall efficiencies of these porphyrins. The higher polarizability is advantageous to facilitate intramolecular photoinduced electron transfer.

Dye Loading Measurements

To better comprehend the adsorption behavior and measure the amount of the adsorbed dye, we performed the measurements of porphyrin densities (Γ) adsorbed on TiO$_2$ surface. The porphyrin densities were determined by measuring the concentrations of the porphyrin solutions desorbed from the dye-coated TiO$_2$ films after being immersed in 0.1 M KOH solution in THF. The saturated Γ values of the porphyrins under study were found as 360 ± 30, 180 ± 30 and 62 ± 10 nmol cm^{-2} for N4, N3S and N3O porphyrins respectively. The dye loadings values are consistent with the overall conversion efficiencies obtained for the studied porphyrins, reported below. We attribute the difference of dye-loading to the different affinity of the dye to the TiO$_2$ surface. The oxaporphyrin which is a more electron-rich porphyrin might decrease the acidity of carboxylic acid and decrease the affinity of N3O to TiO$_2$ surface.

Photovoltaic Measurements

DSSCs based on liquid electrolytes were fabricated using the porphyrins N4, N3S and N3O and tested under AM 1.5 conditions. The photovoltaic parameters for the porphyrins in this study are summarized in Table 3 and the I-V curves of the devices assembled using the porphyrins and measured under standard AM 1.5 G simulated solar conditions are shown in Figure 6.

As seen from the I-V curves, the device using regular free-base porphyrin N4 outperformed those heteroporphyrin-based devices. It obtained the highest efficiency of 3.66% with photocurrent density of 8.82 mA cm^{-2}, open-circuit voltage of 0.57 V, and fill factor of 73%. The thia-

Table 2. Calculated TD-DFT composition in terms of frontier molecular orbitals, excitation energy, and the oscillator strengths of N4, N3S, and N3O

Dyes	State	Composition (%)	E (eV)	λ (nm)	f	D (Debye)
N$_4$	S1	H−1→L (12)	2.05	603.18	0.2321	4.72
		H−1→L+1 (12)				
		H→L (53)				
		H→L+1 (22)				
	S2	H−1→L (24)	2.20	563.23	0.2144	
		H−1→L+1 (6)				
		H→L (29)				
		H→L+1 (41)				
	S3	H−1→L+1 (37)	2.97	417.78	1.1369	
		H→L (9)				
		H→L+2 (46)				
	S4	H−2→L (59)	3.19	388.66	0.2144	
		H−1→L+1 (8)				
		H→L+2 (17)				
N$_3$S	S1	H−1→L (13)	1.99	620.08	0.1509	4.57
		H−1→L+1 (11)				
		H→L (46)				
		H→L+1 (28)				
	S2	H−1→L (20)	2.18	567.41	0.276	
		H−1→L+1 (7)				
		H→L (35)				
		H→L+1 (37)				
	S3	H−4→L (10)	2.91	425.58	0.9903	
		H−1→L+1 (42)				
		H→L (9)				
		H→L+2 (24)				
	S4	H−4→L (59)	3.13	396.39	0.3169	
		H−2→L (24)				
N$_3$O	S1	H−1→L (16)	2.02	613.44	0.1412	4.04
		H−1→L+1 (9)				
		H→L (39)				
		H→L+1 (34)				
	S2	H−1→L (18)	2.19	565.7	0.2903	
		H−1→L+1 (9)				
		H→L (42)				
		H→L+1 (30)				
	S3	H−3→L (6)	2.94	422.15	1.0362	
		H−1→L (9)				
		H−1→L+1 (38)				
		H→L (7)				
		H→L+2 (30)				
	S4	H−4→L (10)	3.11	398.48	0.0522	
		H−2→L (56)				
		H−2→L+1 (22)				

H=HOMO, L=LUMO, H−1=HOMO−1, H−2=HOMO−2, H−3=HOMO−3, H−4=HOMO−4, L+1=LUMO+1, L+2=LUMO+2.

porphyrin N3S gave the photocurrent density of 0.83 mA cm^{-2}, open-circuit voltage of 0.45 V, and fill factor of 58%.

Table 3. Photovoltaic parameters of N4, N3S and N3O dyes

Dye	J_{sc} (mA cm^{-2})	V_{oc} (V)	ff (%)	η (%)
N4	8.82	0.57	73	3.66
N3S	0.83	0.45	58	0.22
N3O	0.06	0.24	50	0.01

The oxaporphyrin N3O obtained the photocurrent density of 0.06 mA cm^{-2}, the open-circuit voltage of 0.24, and fill factor of 50%. These parameters gained the overall conversion efficiencies of 0.22% for N3S and 0.01% for N3O. The enhanced non-radiative internal conversion or intersystem crossing for the heteroporphyrins compared to regular porphyrins might decrease the lifetimes of the excited state and decrease the efficiency of electron injection from the dye molecules to the conduction bands of TiO$_2$. The heavy atom effect of sulfur atom causes faster intersystem crossing rate can be the main reason for the low efficiency of N3S.[16] The incident photon-to-current conversion efficiency (IPCE) spectra (Figure 7) for all the porphyrins are in good agreement with the corresponding absorption spectra on TiO$_2$ which display the characteristic intense absorption in the *Soret* region. The IPCE maximum for regular N4 porphyrin is found to be 50% in between 400-500 nm re-

gion and those for N3S and N3O are found to be 12% and less than 1%, respectively. The ICPE values for N3S porphyrin are surprisingly small and for N3O it is almost negligible in the *Q* band region. The I-V curves under standard AM 1.5 G illumination are in qualitative agreement with the photo-action spectra.

TCSPC Measurements

As shown in Figure 8, the time-correlated single photon counting (TCSPC) data of N4, N3O and N3S adsorbed on Al$_2$O$_3$ or TiO$_2$ films allow the studies of excited state lifetimes when these dyes were excited at Q(0,0) bands. Because of the complicated relaxation processes at the excited state, the lifetimes have been deconvoluted into two or three components using an iterative non-linear deconvolution fitting method and the mean lifetimes (τ_{av}), as shown in Table 4, are obtained from the weighted average of τ_1 and τ_2, two main decaying components presence in the data of all dyes. The mean relaxation lifetime of N4 on non-injecting Al$_2$O$_3$ film is similar to that of N3S, and is longer than that of N3O. The short excited lifetime for N3O on AlO$_3$ implies an extremely fast internal conversion and/or intermolecular energy transfer processes caused by dye-aggregations. As expected the fast electron injections into the TiO$_2$ conduction band after the photo-excitations
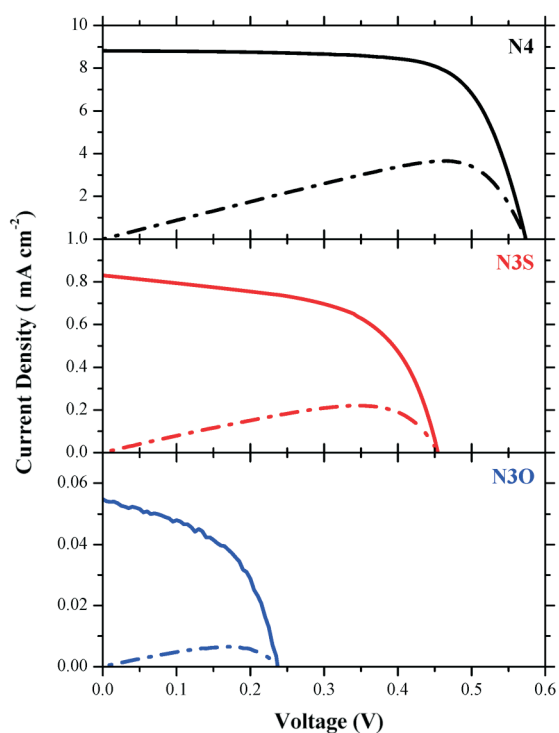

Fig. 6. I-V curves of the DSSCs fabricated with N4, N3S and N3O porphyrins under one sun.
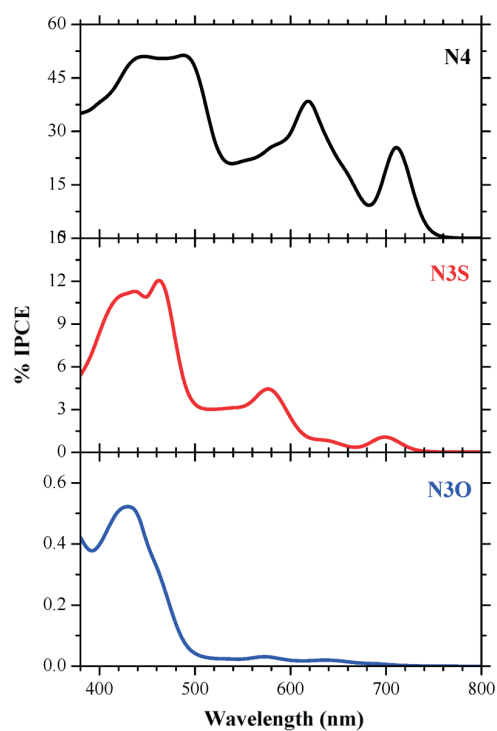

Fig. 7. IPCE spectra of the DSSCs fabricated with N4, N3S and N3O porphyrins.

Table 4. Fluorescence lifetimes and their fractional weights (A_i, normalized to 100%) of emission decays of porphyrin dyes absorbed on either Al_2O_3 or TiO_2

Dye	τ_1/ns (A_1%)	τ_2/ns (A_2%)	τ_3/ns (A_3/%)	Average (τ_{av}/ns)[a]
$N4/TiO_2$	0.194(91)	0.522(9)	-	0.223
$N4/Al_2O_3$	0.275(71)	0.87(25)	2.258(4%)	0.413
$N3S/TiO_2$	0.234(85)	0.606(15)	-	0.290
$N3S/Al_2O_3$	0.354(87)	0.894(13)	-	0.424
$N3O/TiO_2$	0.08(96)	0.465(3)	1.534(1%)	0.091
$N3O/Al_2O_3$	0.12(95)	0.697(4)	3.216(1%)	0.142

[a] Average = $(\tau_1 \times A_1\%) + (\tau_2 \times A_2\%)$

significantly decrease the fluorescence lifetimes for the dyes adsorbed on TiO_2 films and the relative lifetimes reflect the efficiencies of electron injection. It is interesting to note that the difference of fluorescence transients between TiO_2 and Al_2O_3 are more obvious for N4 than for N3O and N3S. The intrinsic rapid fluorescence quenching of N3O as observed on Al_2O_3 film leads to near static lifetimes between N3O adsorbed on TiO_2 and Al_2O_3. Overall, the TCSPC data agree with the trend of efficiencies of electron injection as N4 > N3S >> N3O.
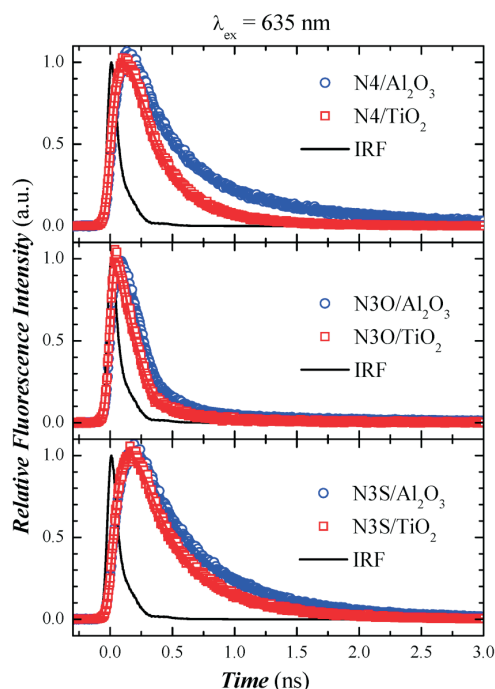

Fig. 8. Picosecond fluorescence transients of the porphyrin sensitizers absorbed on either TiO_2 or Al_2O_3; the fitted lifetimes are summarized in Table 4. (The black curve is instrument response function from picosecond laser source.)

CONCLUSIONS

In summary, three novel free-base porphyrin sensitizers, N4, N3S, and N3O, were synthesized by simple and short routes. It is observed that the alteration of the core atom by group 16 heteroatoms has significant effects on the photophysical as well as photovoltaic properties of the studied porphyrins. The UV-visible spectra of the heteroporphyrins suggest that core-atom modification results in bathochromic enhancement of the absorption bands with the absorption onset reaching the NIR region. The steady-state fluorescence spectra display that the heteroatom substitutions on one of the pyrrolic nitrogens result in faster internal conversion or intersystem crossing which accelerate the non-radiative decay rates. The I-V curves suggest that the photocurrent density and the open-circuit voltage decrease substantially in DSSCs using core-modified porphyrins as the sensitizer. The overall conversion efficiencies of the devices display the order N4 (3.66%) >> N3S (0.22%) > N3O (0.01%). Noticeably, although lower dye loading can decrease the photo-current on N3O based DSSC, the fluorescence lifetimes suggest that poor electron injection caused by rapid excited-state relaxation is the main reason for the poor performance of N3O dye.

EXPERIMENTAL

Materials: All chemicals were obtained from commercial sources and used as received without further purification. All the reactions were carried out under nitrogen atmosphere. Solvents used in the reactions were dried by PureSolv MD 5 system (Innovative Technology, Inc). Flash chromatography was carried out by using basic alumina (63-200 μm, Merck) and silica gel (40-63 μm, Merck). Analytical TLC was performed on Merck silica gel plates. NMR spectra were recorded on a Bruker Avance 400 FT spectrometer. The ESI ion trap mass spectra were measured by a Finnigan MAT LCQ mass spectrometer.

Synthesis: 2-(Hydroxymethyl)-5-[hydroxy(p-tolyl)methyl]thiophene,[17] 2-(hydroxymethyl)-5-[hydroxyl(p-tolyl)methyl]furan,[17] 10,15,20-tris(p-tolyl)porphyrin (**1**),[18] and 4-ethynyl-benzoic acid[19] were synthesized by following literature procedures.

10,15,20-Tris(p-tolyl)-21-thiaporphyrin (2): In a 250 mL one-necked round-bottomed flask fitted with a N_2 gas bubbler, the thiophene diol (335 mg, 1.43 mmol), pyrrole (320 μL, 4.70 mmol), and p-tolualdehyde (350 μL, 2.91 mmol) were dissolved in CH_2Cl_2 (150 mL). After purging the solution with N_2 for 15 min, the condensation reaction of the diol, aldehyde and pyrrole was initiated at room temperature by addition of a catalytic

amount of BF$_3$/OEt$_2$ (100 μL). After stirring for 1 h, DDQ (240 mg, 1.07 mmol) was added and the reaction mixture was stirred at room temperature in air for an additional hour. The solvent was removed on a rotary evaporator. The crude product was purified by silica gel column chromatography using hexane/CH$_2$Cl$_2$ (1:1) as the eluent to afford a purple solid (62 mg, 7%) after solvent removal. ^{1}H NMR (400 MHz, CDCl$_3$) δ, ppm: -2.82 (s, 1H, NH), 2.72 (s, 9H, CH$_3$), 7.54-7.67 (m, 6H, *m*-tolyl), 8.07-8.19 (m, 6H, *o*-tolyl), 8.64 (d, 1H, *J* = 4.44 Hz, β-pyrrole), 8.74 (m, 2H, β-pyrrole), 8.99 (s, 2H, β-pyrrole), 9.05 (d, 1H, *J* = 4.32 Hz, β-pyrrole), 9.89 (d, 1H, *J* = 5.12 Hz, β-thiophene), 10.02 (d, 1H, *J* = 5.04 Hz, β-thiophene), 10.67 (s, 1H, *meso*); HRMS-ESI: *m/z* calcd for C$_{41}$H$_{32}$N$_3$S: 598.2317, found 598.2318 [M+H]$^+$.

10,15,20-Tris(p-tolyl)-21-oxaporphyrin (3): In a 250 mL one-necked round-bottomed flask fitted with a N$_2$ gas bubbler, the furan diol (500 mg, 2.29 mmol), pyrrole (500 μL, 7.31 mmol), and *p*-tolualdehyde (590 μL, 5.06 mmol) were dissolved in CH$_2$Cl$_2$ (200 mL). After purging with N$_2$ for 15 min, the condensation reaction of the diol, aldehyde, and pyrrole was initiated at room temperature by the addition of a catalytic amount of BF$_3$/OEt$_2$ (60 μL, 0.23 mmol). After stirring for 1 h, DDQ (520 mg, 2.32 mmol) was added and the reaction mixture was stirred at room temperature in air for an additional hour. The solvent was removed on a rotary evaporator. The crude product was purified by basic alumina column chromatography using hexane/CH$_2$Cl$_2$ (1:1) and then CH$_2$Cl$_2$ as the eluent to afford a purple solid (67 mg, 5%) after solvent removal. ^{1}H NMR (400 MHz, CDCl$_3$) δ, ppm: 2.74 (s, 9H, CH$_3$), 7.60 (m, 6H, *m*-tolyl), 8.12 (m, 6H, *o*-tolyl), 8.68 (d, 2H, β-pyrrole), 8.89 (s, 1H, β-pyrrole), 8.95 (d, 2H, β-pyrrole), 9.15 (s, 1H, β-pyrrole), 9.39 (s, 1H, β-furan), 9.71 (s, 1H, β-furan), 10.17 (s, 1H, meso); HRMS-ESI: *m/z* calcd for C$_{41}$H$_{32}$N$_3$O: 582.2545, found 582.2542 [M+H]$^+$.

5-Bromo-10,15,20-tris(p-tolyl)porphyrin (4): To a stirred solution of 10,15,20-tris(*p*-tolyl)porphyrin (1) (200 mg, 0.34 mmol) in chloroform (50 mL) at room temperature, *N*-bromosuccinimide (NBS) (73 mg, 0.41 mmol) was added. The progress of the reaction was monitored by TLC and absorption spectroscopy. After complete consumption of the starting porphyrin as confirmed by TLC, the reaction was quenched with acetone (10 mL) and the solvent was removed on a rotary evaporator under vacuum. The crude reaction mixture was purified by silica gel column chromatography with hexane/CH$_2$Cl$_2$ (70:30) as the eluent and the pure brominated porphyrin were obtained as a purple solid in 70% yield (157 mg, 0.24 mmol). ^{1}H NMR (400 MHz, CDCl$_3$) δ, ppm: -2.74 (s, 2H, NH), 2.69 (s, 3H, CH$_3$), 2.71 (s, 6H, CH$_3$), 7.53-7.58 (m, 6H, *m*-tolyl), 8.05-8.08 (m, 6H, *o*-tolyl), 8.81 (s, 4H, β-pyrrole), 8.91 (d, 2H, *J* = 4.7 Hz, β-pyrrole), 9.65 (d, 2H, *J* = 4.8 Hz,

β-pyrrole); HRMS-ESI: *m/z* calcd for C$_{41}$H$_{32}$N$_4$Br: 659.1810, found 659.1806 [M+H]$^+$. **5-Bromo-10,15,20-tris(p-tolyl)-21-thiaporphyrin (5):** To a solution of 10,15,20-tris(p-tolyl)-21-thiaporphyrin (2) (137 mg, 0.23 mmol) in dry dichloromethane (25 mL) in a 50 mL round-bottomed flask was added NBS (49 mg, 0.28 mmol) at 0 °C and the reaction mixture was stirred at room temperature for 30 min. After complete consumption of the starting thiaporphyrin as confirmed by TLC, the reaction was quenched with acetone and the solvent was removed with a rotary evaporator under vacuum. The crude compound was subjected to silica gel column chromatography using hexane/CH$_2$Cl$_2$ (2:1) as the eluent and the pure bromoporphyrin was isolated as a purple solid (118 mg, 77%) after drying. ^{1}H NMR (400 MHz, CDCl$_3$) δ, ppm: -2.59 (s, 1H, NH), 2.70 (s, 9H, CH$_3$), 7.52-7.65 (m, 6H, *m*-tolyl), 8.03-8.13 (m, 6H, *o*-tolyl), 8.58 (d, 1H, *J* = 4.52 Hz, β-pyrrole), 8.64 (m, 2H, β-pyrrole), 8.91 (d, 2H, *J* = 1.80 Hz, β-pyrrole), 9.30 (d, 1H, *J* = 4.56 Hz, β-pyrrole), 9.83 (d, 1H, *J* = 5.24 Hz, β-thiophene), 10.19 (d, 1H, *J* = 5.28 Hz, β-thiophene); HRMS-ESI: *m/z* calcd for C$_{41}$H$_{31}$BrN$_3$S: 676.1422, found 676.1417 [M+H]$^+$. **5-Bromo-10,15,20-tris(p-tolyl)-21-oxaporphyrin (6):** To a solution of 10,15,20-tris(p-tolyl)-21-oxaporphyrin (3) (58 mg, 0.1 mmol) in dry CH$_2$Cl$_2$ (10 mL) in a 50 mL round-bottomed flask was added NBS (22 mg, 0.12 mmol) at 0 °C and then the reaction mixture was stirred at room temperature for 30 min. The progress of the reaction was monitored by TLC. After complete consumption of the starting oxaporphyrin as confirmed by TLC, the reaction was quenched with acetone and the solvent was removed with a rotary evaporator under vacuum. The crude compound was subjected to silica gel column chromatography with acetone/CH$_2$Cl$_2$ (1:9) as the eluent and the pure bromoporphyrin was collected as a purple solid (52 mg, 78 %) after drying. ^{1}H NMR (400 MHz, CDCl$_3$) δ, ppm: 2.71 (m, 9H, CH$_3$), 7.54-7.58 (m, 6H, *m*-tolyl), 8.03-8.07 (m, 6H, *o*-tolyl), 8.52 (d, 1H, *J* = 4.64 Hz, β-pyrrole), 8.59 (d, 1H, *J* = 4.64 Hz, β-pyrrole), 8.70 (d, 1H, *J* = 4.68 Hz, β-pyrrole), 8.86 (s, 2H, β-pyrrole), 9.31 (d, 1H, *J* = 4.88 Hz, β-pyrrole), 9.51 (d, 1H, *J* = 4.68 Hz, β-furan), 10.06 (d, 1H, *J* = 4.92 Hz, β-furan); HRMS-ESI: *m/z* calcd for C$_{41}$H$_{31}$BrN$_3$O: 660.1650, found 660.1652 [M+H]$^+$. **5-(4-Ethynyl-benzoicacid)-10,15,20-tris(p-tolyl)porphyrin (7) [N4]:** A mixture of 4-ethynylbenzoic acid (55 mg, 0.38 mmol) and 5-bromo-10,15,20-tris(*p*-tolyl)porphyrin (50 mg, 0.076 mmol) in dry THF (5 mL) and Et$_3$N (5 mL) was degassed with N$_2$ for 10 min, and then Pd$_2$(dba)$_3$ (27 mg, 0.03 mmol) and AsPh$_3$ (58 mg, 0.19 mmol) were added to the mixture. The solution was stirred at room temperature for 12 h under N$_2$. The solvent was removed in vacuo, and the residue was purified by silica gel column chromatography with CH$_2$Cl$_2$/methanol = 9/1 as the eluent to give purple

solid (31 mg, 56% yield) after drying. Mp > 300 °C; ^{1}H NMR (400 MHz, THF-d8) δ, ppm: -2.22 (s, 2H, NH), 2.68 (s, 3H, CH_3), 2.71 (s, 6H, CH_3), 7.57-7.63 (m, 6H, m-tolyl), 8.04-8.11 (m, 6H, o-tolyl), 8.16 (d, 2H, J = 8.3 Hz, Ph), 8.24 (d, 2H, J = 8.4 Hz, Ph), 8.76 (s, 4H, β-pyrrole), 8.94 (d, 2H, J = 4.7 Hz, β-pyrrole), 9.78 (d, 2H, J = 4.7 Hz, β-pyrrole) ppm; ^{13}C NMR (125 MHz, THF-d8) δ: 20.55, 94.41, 95.91, 98.02, 121.29, 122.33, 124.43, 124.92, 127.30, 127.42, 128.12, 129.03, 129.84, 130.71, 131.21, 131.43, 131.68, 134.14, 134.30, 137.52, 138.83, 139.11, 166.19 ppm; IR (Neat, cm[-1]): 3312, 1684, 1603, 1424, 1312, 1292, 1174, 965, 794; UV-vis (THF) λ_{max}/nm (ε/10^3 M^{-1}cm^{-1}) = 433 (245), 534 (11), 575 (31), 610 (4), 668 (11); HRMS-ESI: m/z calcd for $C_{50}H_{37}N_4O_2$: 725.2917, found 725.2919 [M+H][+]. **5-(4-Ethynylbenzoicacid)-10,15,20-tris(p-tolyl)-21-thiaporphyrin (8) [N3S]:** 5-Bromo-10,15,20-tris(p-tolyl)-21-thiaporphyrin (5) (100 mg, 0.15 mmol), Pd_2(dba)_3 (55 mg, 0.06 mmol), AsPh_3 (113 mg, 0.37 mmol) and 4-ethynyl benzoic acid (26 mg, 0.18 mmol) were added to a 100 ml round bottom flask and the flask is attached to high vacuum for 30 min. A flow of N_2 gas was then flushed for 15 min before dry THF (40 mL) and triethylamine (10 mL) were added. The reaction mixture was stirred under N_2 at room temperature until completion of the reaction as monitored by TLC. The solvent was removed under vacuum and the crude product was purified by silica gel column chromatography using 5% methanol/CH_2Cl_2 as the eluent to isolate the pure product as a purple solid (99 mg, 90%) after drying. Mp > 300 °C; ^{1}H NMR (400 MHz, DMSO-d6) δ, ppm: -2.31 (s, 1H, NH), 2.67 (s, 9H, CH_3), 7.61-7.74 (m, 6H, m-tolyl), 8.04-8.16 (m, 6H, o-tolyl), 8.19 (d, 2H, Ph), 8.27 (d, 2H, Ph), 8.46 (d, 1H, β-pyrrole), 8.58 (m, 2H, β-pyrrole), 8.90 (s, 2H, β-pyrrole), 9.44 (d, 1H, β-pyrrole), 9.84 (d, 1H, β-thiophene), 10.48 (d, 1H, β-thiophene) ppm; ^{13}C NMR (100 MHz, DMSO-d6) δ: 21.01, 92.07, 98.29, 108.29, 124.80, 125.66, 126.76, 127.49, 127.60, 128.64, 129.15, 129.45, 129.76, 130.86, 131.96, 132.70, 133.12, 133.58, 133.91, 135.51, 136.03, 136.66, 137.63, 137.79, 138.04, 138.23, 138.38, 138.89, 145.28, 149.18, 153.70, 157.15, 157.95, 166.72 ppm; IR (Neat, cm[-1]): 3326, 1684, 1603, 1429, 1313, 1293, 1176, 967, 795; UV-vis (THF) λ_{max}/nm (ε/10^3 M^{-1}cm^{-1}) = 442 (257), 529 (17), 571 (37), 633 (5), 696 (9); HRMS-ESI: m/z calcd for $C_{50}H_{36}N_3O_2S$: 742.2528, found 742.2535 [M+H][+]. **5-(4-Ethynylbenzoicacid)-10,15,20-tris(p-tolyl)-21-oxaporphyrin (9)[N3O]:** 5-Bromo-10,15,20-tris(p-tolyl)-21-oxaporphyrin (6) (52 mg, 0.08 mmol), Pd_2(dba)_3 (28 mg, 0.03 mmol), AsPh_3 (60 mg, 0.19 mmol) and 4-ethynyl benzoic acid (17 mg, 0.12 mmol) were added to a 100 ml round bottom flask and the flask is attached to high vacuum for 30 min. N_2 gas was then flushed for 15 min before dry THF (20 mL) and triethylamine (5 mL) were added. The reaction mixture was

stirred under N_2 at room temperature until completion of the reaction as monitored by TLC. The solvent was removed under pressure and the crude product was purified by silica gel column chromatography using 5% methanol/CH_2Cl_2 as eluent to afford the pure product as a purple solid (29 mg, 51%). Mp > 300 °C; ^{1}H NMR (400 MHz, THF-d8) δ: 2.69 (m, 9H, CH_3), 7.56-7.62 (m, 6H, m-tolyl), 8.01-8.17 (m, 6H, o-tolyl), 8.15 (d, 2H, J = 8.20 Hz, Ph), 8.24 (d, 2H, J = 8.24 Hz, Ph), 8.38 (d, 1H, J = 4.60 Hz, β-pyrrole), 8.44 (d, 1H, J = 4.56 Hz, β-pyrrole), 8.64 (d, 1H, J = 4.60 Hz, β-pyrrole), 8.78 (s, 2H, β-pyrrole), 9.32 (d, 1H, J = 4.80 Hz, β-pyrrole), 9.56 (d, 1H, J = 4.56 Hz, β-furan), 10.15 (d, 1H, J = 4.76 Hz, β- furan) ppm; ^{13}C NMR (125 MHz, THF-d8) δ: 21.55, 94.17, 97.23, 98.88, 120.43, 125.12, 126.03, 127.27, 127.73, 128.34, 128.39, 128.60, 128.76, 130.00, 130.31, 130.43, 130.75, 131.75, 135.11, 135.27, 135.76, 136.02, 138.50, 138.77, 139.60, 139.83, 140.08, 140.62, 155.67, 157.17, 157.66, 157.84, 157.87, 168.98 ppm; IR (Neat, cm[-1]): 3233, 1707, 1603, 1462, 1376, 1258, 1181, 967, 798; UV-vis (THF) λ_{max}/nm (ε/10^3 M^{-1}cm^{-1}) = 436 (247), 525 (9), 565 (19), 629 (3), 691 (5); HRMS-ESI: m/z calcd for $C_{50}H_{36}N_3O_3$: 726.2757, found 726.2759 [M+H][+].

Optical Spectroscopy: Transmittance and reflection UV–visible absorption spectra of the porphyrins in tetrahydrofuran (THF) and adsorbed on TiO_2 electrodes, respectively, were recorded on a JASCO V-670 UV–vis/NIR spectrophotometer. Steady-state fluorescence spectra were acquired by using a Varian Cary Eclipse fluorescence spectrophotometer.

Cyclic Voltammetry: The cyclic voltammetry measurements of the porphyrins were carried out on CHI 621B electrochemical analyzer (CH Instruments, Austin, TX, USA) in degassed THF containing 0.1 M tetrabutylammonium hexafluorophosphate (Bu_4NPF_6) as the supporting electrolyte. The cell assembly consists of a glossy carbon as the working electrode, a silver wire as the pseudo-reference electrode, and a platinum wire as the auxiliary electrode. The scan rate for all measurements was fixed at 50 mV/sec. A ferrocene[+1/0] redox couple was used as the internal standard and the potential values obtained in reference to the silver electrode were converted to the vacuum scale.

Theoretical Calculations: The DFT and TD-DFT calculations were performed with Gaussian 09 package to study the distribution of electron density of the frontier molecular orbitals and the photo-excitation transitions.[20] All ground state geometries of studied porphyrins were optimized in the gas phase by the hybrid B3LYP functional and the 6-31G basis set, and the TD-DFT calculations were based on the same functional and basis set. The molecular orbitals were visualized by the Chemoffice software.

Photovoltaic Measurements: To characterize the photovoltaic performance of the DSSC devices, fluorine-doped tin ox-

ide glass (FTO; 6-8 Ω/sq, Pilkington Tec-7, USA, thickness 2.2 mm) plates were washed with a soap solution in an ultrasonic bath for 10 min, and then rinsed with deionized (DI) water and methanol. The FTO glass plates were immersed in 40 mM aqueous $TiCl_4$ at 70 °C for 30 min and washed with DI water and methanol. A transparent nanocrystalline layer was prepared on the FTO glass plate by repeated screen printing with TiO_2 paste (Solaronix, 15-20 nm Ti-Nanoxide T/SP), then drying for 2 h at room temperature. The TiO_2 electrodes were gradually heated at 110 °C for 1 h and 450 °C for 1 h. The resulting layer was composed of a ~11 μm thickness, measured by DekTak 150 stylus profiler. Finally a scattering layer containing >100 nm anatase particles (Solaronix, Ti-Nanoxide R/SP) was deposited by screen printing and then dried at room temperature for 2 h. The FTO glass plates were again immersed in 40 mM aqueous $TiCl_4$ at 70 °C for 30 min and washed with DI water and methanol. The TiO_2 electrodes were gradually heated at 110 °C for 1 h and 450 °C for 1 h. The porphyrin/TiO_2 layer was served as a working electrode (anode). We immersed the TiO_2 coated FTO (TiO_2 active size 0.4 × 0.4 cm^2) films in a THF solution containing porphyrins ($1 × 10^{-4}$ M) at 40 °C for 2 h. The FTO glass plate used as cathode was coated with Pt particles by using the thermal platinum nano-cluster catalyst method. The Pt catalyst was deposited from a precursor solution composed of 5 mM solution of hexachloroplatinic acid in anhydrous isopropanol. The precursor solution was spin-coated on FTO glass (10 L/cm^2) and dried in air for 3 min. Coated Pt electrode was placed in an oven and temperature was gradually increased to 360 °C and kept under 360 °C for 15 min. To fabricate the DSSC device, the two electrodes were assembled into a sandwich-type cell. The thin layer of electrolyte was introduced into the space between the two electrodes. A typical redox electrolyte containing lithium iodide (LiI, 0.1 M), diiodine (I_2, 0.05 M), 1,2-dimethyl-3-propylimidazolium iodide (DMII, 0.5 M), and 0.5 M 4-*tert*-butylpyridine in dry acetonitrile. The photoelectrochemical characterizations of the solar cells were carried out by using an Oriel Class-A solar simulator (Oriel 91195A, Newport Corp.). Photocurrent and voltage curves were recorded with a potentiostat/galvanostat (CHI 650B, CH Instruments, Inc., USA) at a light intensity of one-sun irradiation calibrated by an Oriel reference solar cell (Oriel 91150, Newport Corp.). The incident photon-to-current conversion efficiency (IPCE) measurements were carried out with a monochromator (Oriel 74100) at short circuit conditions.

TCSPC Measurements: Fluorescence transients were recorded with a time-correlated single-photon counting (TCSPC) system (FluoTime 200, PicoQuant) with the picosecond laser source (PicoQuant) for excitation at λ_{ex} = 635 nm. The excitation pulse was focused onto a rotating sample holder with a lens. A lens collected emission emitted from the sample at a right angle. An iris attenuated the intensity of the detected signal; the polarization of the detected emission relative to the excitation laser pulse was set at 54.7° with a polarizer. A double monochromator of a subtractive type compensated the group-velocity dispersion of emission and selected the detection wavelength; the resolution was 8 nm with a slit of width 1 mm. A micro-channel plate photomultiplier was connected to a computer with a TCSPC-module card (SPC-630, Becker & Hickl GmbH) for data acquisition. The FWHM of the instrument response function (IRF) was typically 80 ps, measured with scattered light at the laser excitation wavelength.

REFERENCES

1. (a) O'Regan, B.; Gratzel, M. *Nature* **1991**, *353*, 737; (b) Burschka, J.; Pellet, N.; Moon, S. J.; Humphry-Baker, R.; Gao, P.; Nazeeruddin, M. K.; Gratzel, M. *Nature* **2013**, *499*, 316; (c) Goncalves, L. M.; de Zea Bermudez, V.; Ribeiro, H. A.; Mendes, A. M. *Energy Environ. Sci.* **2008**, *1*, 655; (d) Grätzel, M. *Acc. Chem. Res.* **2009**, *42*, 1788; (e) Hagfeldt, A.; Boschloo, G.; Sun, L.; Kloo, L.; Pettersson, H. *Chem. Rev.* **2010**, *110*, 6595.

2. (a) Imahori, H.; Umeyama, T.; Ito, S. *Acc. Chem. Res.* **2009**, *42*, 1809; (b) Mishra, A.; Fischer, M. K. R.; Bäuerle, P. *Angew. Chem. Int. Ed.* **2009**, *48*, 2474; (c) Martinez-Diaz, M. V.; de la Torre, G.; Torres, T. *Chem. Commun.* **2010**, *46*, 7090.

3. (a) Muthiah, C.; Taniguchi, M.; Kim, H.-J.; Schmidt, I.; Kee, H. L.; Holten, D.; Bocian, D. F.; Lindsey, J. S. *Photochem. Photobiol.* **2007**, *83*, 1513; (b) Lee, C. Y.; She, C.; Jeong, N. C.; Hupp, J. T. *Chem. Commun.* **2010**, *46*, 6090; (c) He, H.; Gurung, A.; Si, L. *Chem. Commun.* **2012**, *48*, 5910.

4. (a) Rochford, J.; Chu, D.; Hagfeldt, A.; Galoppini, E. *J. Am. Chem. Soc.* **2007**, *129*, 4655; (b) Lin, C.-Y.; Lo, C.-F.; Luo, L.; Lu, H.-P.; Hung, C.-S.; Diau, E. W.-G. *J. Phys. Chem. C* **2008**, *113*, 755.

5. (a) Nazeeruddin, M. K.; Humphry-Baker, R.; Officer, D. L.; Campbell, W. M.; Burrell, A. K.; Grätzel, M. *Langmuir* **2004**, *20*, 6514; (b) Gervaldo, M.; Fungo, F.; Durantini, E. N.; Silber, J. J.; Sereno, L.; Otero, L. *J. Phys. Chem. B* **2005**,

109, 20953; (c) Alibabaei, L.; Wang, M.; Giovannetti, R.; Teuscher, J.; Di Censo, D.; Moser, J.-E.; Comte, P.; Pucciarelli, F.; Zakeeruddin, S. M.; Gratzel, M. *Energy Environ. Sci.* **2010**, *3*, 956; (d) Xiang, N.; Zhou, W.; Jiang, S.; Deng, L.; Liu, Y.; Tan, Z.; Zhao, B.; Shen, P.; Tan, S. *Sol. Energy Mater. Sol. Cells* **2011**, *95*, 1174.

6. Li, L.-L.; Diau, E. W.-G. *Chem. Soc. Rev.* **2013**, *42*, 291.

7. Han, L.; Islam, A.; Chen, H.; Malapaka, C.; Chiranjeevi, B.; Zhang, S.; Yang, X.; Yanagida, M. *Energy Environ. Sci.* **2012**, *5*, 6057.

8. Yella, A.; Lee, H.-W.; Tsao, H. N.; Yi, C.; Chandiran, A. K.; Nazeeruddin, M. K.; Diau, E. W.-G.; Yeh, C.-Y.; Zakeeruddin, S. M.; Grätzel, M. *Science* **2011**, *334*, 629.

9. (a) Campbell, W. M.; Jolley, K. W.; Wagner, P.; Wagner, K.; Walsh, P. J.; Gordon, K. C.; Schmidt-Mende, L.; Nazeeruddin, M. K.; Wang, Q.; Grätzel, M.; Officer, D. L. *J. Phys. Chem. C* **2007**, *111*, 11760; (b) Mozer, A. J.; Griffith, M. J.; Tsekouras, G.; Wagner, P.; Wallace, G. G.; Mori, S.; Sunahara, K.; Miyashita, M.; Earles, J. C.; Gordon, K. C.; Du, L.; Katoh, R.; Furube, A.; Officer, D. L. *J. Am. Chem. Soc.* **2009**, *131*, 15621; (c) Bessho, T.; Zakeeruddin, S. M.; Yeh, C.-Y.; Diau, E. W.-G.; Grätzel, M. *Angew. Chem. Int. Ed.* **2010**, *49*, 6646; (d) Kira, A.; Matsubara, Y.; Iijima, H.; Umeyama, T.; Matano, Y.; Ito, S.; Niemi, M.; Tkachenko, N. V.; Lemmetyinen, H.; Imahori, H. *J. Phys. Chem. C* **2010**, *114*, 11293; (e) Mai, C.-L.; Huang, W.-K.; Lu, H.-P.; Lee, C.-W.; Chiu, C.-L.; Liang, Y.-R.; Diau, E. W.-G.; Yeh, C.-Y. *Chem. Commun.* **2010**, *46*, 809; (f) Chang, Y.-C.; Wang, C.-L.; Pan, T.-Y.; Hong, S.-H.; Lan, C.-M.; Kuo, H.-H.; Lo, C.-F.; Hsu, H.-Y.; Lin, C.-Y.; Diau, E. W.-G. *Chem. Commun.* **2011**, *47*, 8910; (g) Ball, J. M.; Davis, N. K. S.; Wilkinson, J. D.; Kirkpatrick,

J.; Teuscher, J.; Gunning, R.; Anderson, H. L.; Snaith, H. J. *RSC Advances* **2012**, *2*, 6846.

10. Latos-Grazynski, L. *The Porphyrin Handbook Vol. 2*; Academic Press: New York, 2010.

11. (a) Hung, C.-H.; Lin, C.-Y.; Lin, P.-Y.; Chen, Y.-J. *Tetrahedron Lett.* **2004**, *45*, 129; (b) Chuang, C.-H.; Ou, C.-K.; Liu, S.-T.; Kumar, A.; Ching, W.-M.; Chiang, P.-C.; dela Rosa, M. A. C.; Hung, C.-H. *Inorg. Chem.* **2011**, *50*, 11947; (c) Ambre, R.; Yu, C.-Y.; Mane, S. B.; Yao, C.-F.; Hung, C.-H. *Tetrahedron* **2011**, *67*, 4680.

12. Mane, S. B.; Hu, J.-Y.; Chang, Y.-C.; Luo, L.; Diau, E. W.-G.; Hung, C.-H. *Chem. Commun.* **2013**, *49,* 6882-6884.

13. (a) Chmielewski, P. J.; Latos-Grażyñski, L. *Coord. Chem. Rev.* **2005**, *249*, 2510; (b) Gupta, I.; Ravikanth, M. *Coord. Chem. Rev.* **2006**, *250*, 468; (c) Arnold, L.; Müllen, K. *J. Porphyrins Phthalocyanines* **2011**, *15*, 757.

14. Xie, Y.; Joshi, P.; Ropp, M.; Galipeau, D.; Zhang, L.; Fong, H.; You, Y.; Qiao, Q. *J. Porphyrins Phthalocyanines* **2009**, *13*, 903.

15. Ha, J.-H.; Ko, S.; Lee, C.-H.; Lee, W.-y.; Kim, Y.-R. *Chem. Phys. Lett.* **2001**, *349*, 271.

16. Ambre, R.; Chen, K.-B.; Yao, C.-F.; Luo, L.; Diau, E. W.-G.; Hung, C.-H. *J. Phys. Chem. C* **2012**, *116*, 11907.

17. Punidha, S.; Agarwal, N.; Burai, R.; Ravikanth, M. *Eur. J. Org. Chem.* **2004**, *2004*, 2223.

18. Horn, S.; Senge, M. O. *Eur. J. Org. Chem.* **2008**, *2008*, 4881.

19. Wright, A. T.; Song, J. D.; Cravatt, B. F. *J. Am. Chem. Soc.* **2009**, *131*, 10692.

20. Frisch, M. J. Gaussian 09, Revision A.1 Gaussian, Inc.: Wallingford CT 2009.